Human Molecular Genetics, 2020, Vol. 29, No. 17 2855–2871

doi: 10.1093/hmg/ddaa173
Advance Access Publication Date: 7 August 2020
General Article

GENERAL ARTICLE

DOCK3 is a dosage-sensitive regulator of skeletal muscle and Duchenne muscular dystrophy-associated pathologies

Andrea L. Reid[1,†], Yimin Wang[1,†], Adrienne Samani[1], Rylie M. Hightower[1,2], Michael A. Lopez[1,2], Shawn R. Gilbert[3], Lara Ianov[4], David K. Crossman[5], Louis J. Dell'Italia[6,7,8], Douglas P. Millay[9,10], Thomas van Groen[8], Ganesh V. Halade[11] and Matthew S. Alexander[1,2,4,5,*]

[1]Division of Neurology, Department of Pediatrics, The University of Alabama at Birmingham and Children's of Alabama, Birmingham, AL 35294, USA, [2]UAB Center for Exercise Medicine, Birmingham, AL 35294, USA, [3]Department of Orthopedic Surgery, The University of Alabama at Birmingham, Birmingham, AL 35294, USA, [4]Civitan International Research Center, The University of Alabama at Birmingham, Birmingham, AL 35294, USA, [5]Department of Genetics, The University of Alabama at Birmingham, Birmingham, AL 35294, USA, [6]Birmingham Veteran Affairs Medical Center, Birmingham, AL 35233, USA, [7]Division of Cardiovascular Disease, Department of Medicine, The University of Alabama at Birmingham, Birmingham, AL 35294, USA, [8]Department of Cell, Developmental, and Integrative Biology, The University of Alabama at Birmingham, Birmingham, AL 35294, USA, [9]Division of Molecular Cardiovascular Biology, Cincinnati Children's Hospital Medical Center, Cincinnati, OH 45229, USA, [10]Department of Pediatrics, University of Cincinnati College of Medicine, Cincinnati, OH 45267, USA and [11]Division of Cardiovascular Sciences, Department of Medicine, University of South Florida, Tampa, FL 33602, USA

*To whom correspondence should be addressed at: University of Alabama at Birmingham, Children's of Alabama, 1918 University Blvd. MCLM 464 Box 96, Birmingham, AL 35294, USA. Tel: 205-934-7790; Fax: 205-996-0965; Email: malexander@peds.uab.edu

Abstract

DOCK3 is a member of the DOCK family of guanine nucleotide exchange factors that regulate cell migration, fusion and viability. Previously, we identified a dysregulated miR-486/DOCK3 signaling cascade in dystrophin-deficient muscle, which resulted in the overexpression of *DOCK3*; however, little is known about the role of DOCK3 in muscle. Here, we characterize the functional role of DOCK3 in normal and dystrophic skeletal muscle. Utilizing *Dock3* global knockout (*Dock3* KO) mice, we found that the haploinsufficiency of *Dock3* in Duchenne muscular dystrophy mice improved dystrophic muscle pathologies; however, complete loss of *Dock3* worsened muscle function. Adult *Dock3* KO mice have impaired muscle function and *Dock3* KO myoblasts are defective for myogenic differentiation. Transcriptomic analyses of *Dock3* KO muscles reveal a decrease in myogenic factors and pathways involved in muscle differentiation. These studies identify *DOCK3* as a novel modulator of muscle health and may yield therapeutic targets for treating dystrophic muscle symptoms.

[†]Co-first author.

Received: April 30, 2020. **Revised:** July 7, 2020. **Accepted:** July 29, 2020

Graphical Abstract

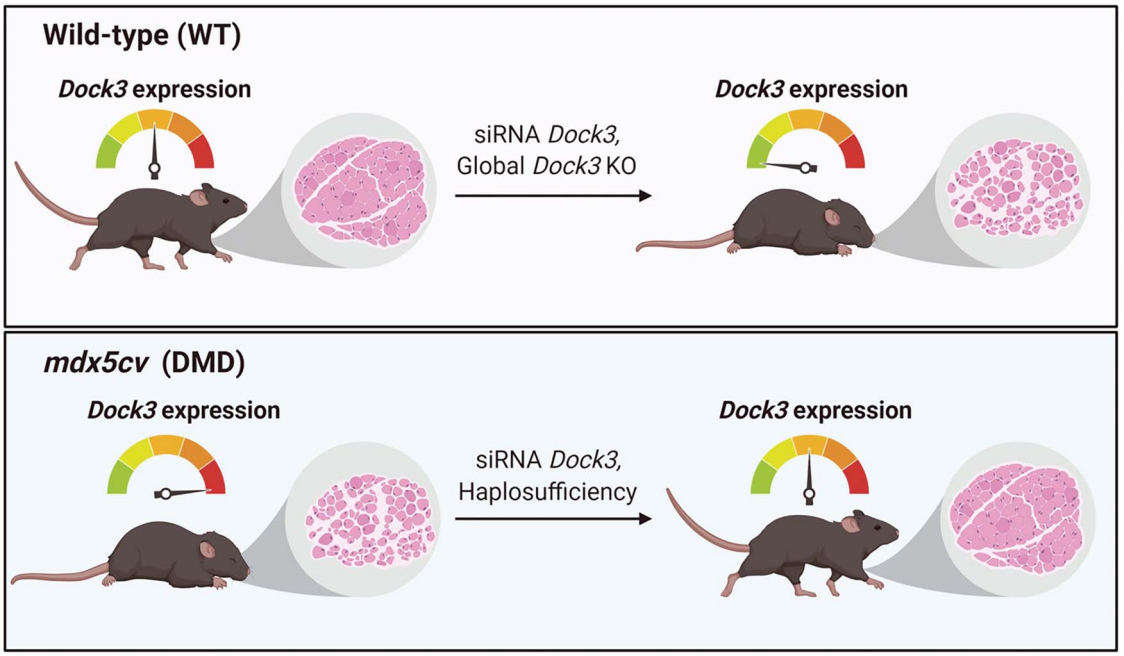

Introduction

Skeletal muscle formation requires a complex coordination of a myriad of signaling factors and cell populations to efficiently form mature myofibers capable of generating muscle force. Duchenne muscular dystrophy (DMD) is an X-linked neuromuscular disorder caused by pathogenic mutations in the *DYSTROPHIN* gene resulting in the lack of functional dystrophin protein. This dystrophin-deficiency results in a degradation of the link between filamentous actin and the extracellular matrix predisposing to structural damage. In DMD patients, after the loss of ambulation, their skeletal muscles begin to progressively deteriorate and are replaced with adipocytes, inflammatory cells and necrotic tissue. While the dystrophin protein has been thought of as a classical muscle structural protein, recent evidence suggests that it also plays a significant role in the regulation of various cellular signaling pathways involved in dystrophic pathology (1–5).

The DOCK (dedicator of cytokinesis) family of proteins functions as key signaling factors that regulate cellular migration, fusion and survival in different cell and tissue types (6). DOCK1 and DOCK5 have been shown to play key roles in myoblast fusion through CRK1/MAPK14 protein interactions (7,8). Additional studies have demonstrated that DOCK3 and DOCK4 activity can regulate key downstream pathways such as Sonic hedgehog to regulate axonal guidance and RAC1 activation (9). DOCK3 (previously called MOCA or modifier of cell adhesion) was shown to be essential for normal neuronal function, and *Dock3* global knockout (KO) mice develop plaques in the brain (10). Human patients with loss-of-function *DOCK3* variants develop intellectual disability, ataxia and developmental delay and have low muscle tone from birth (11–13). There is strong genetic evidence that the disease severity of patients with *DOCK3* pathogenic variants is linked to the degree of which DOCK3 can activate RAC1 signaling as a guanine nucleotide exchange factor (GEF) protein (13). Previously, we identified a muscle-enriched microRNA, miR-486, as a regulator of dystrophin-deficient skeletal muscle pathology in mice and human muscle biopsies through its negative regulation of *DOCK3* mRNA expression levels (14,15). We hypothesized that DOCK3 may be a direct regulator of muscle function and that its dysregulation in DMD may play significant downstream consequences in the progression of the disease. We assessed the roles of DOCK3 in DMD pathology in both zebrafish and mouse models of the disease. We analyzed *Dock3* KO mouse muscles and found significant perturbations in muscle integrity and function. Furthermore, *Dock3* KO mouse muscle cells were analyzed for their ability to proliferate, differentiate and viability in culture. Transcriptomic analyses of *Dock3* KO tibialis anterior (TA) muscles revealed a significant downregulation of several muscle pathways including the fusogen myomixer (*Mymx*), also referred to as myomerger or minion (16–18). This work demonstrates the critical role of DOCK3 in normal myogenesis and a gene-dosing effect of DOCK3 expression levels on dystrophin-deficient muscle health.

Results

Dock3 gene expression is upregulated in dystrophic muscles

We first aimed to assess endogenous *Dock3* gene expression levels in normal and dystrophin-deficient muscle. Previously, we established *DOCK3* as an mRNA target of miR-486, a muscle-enriched miRNA whose expression is reduced in with dystrophic disease progression (14). We evaluated *Dock3* gene expression in our DMD mouse model, *mdx*^{5cv}, and compared with wild-type (WT) (*C57BL/6J* strain) aged-matched male mice. The *mdx*^{5cv} mice have significantly fewer revertant dystrophic fibers, increased muscle weakness and an overall greater dystrophic pathology than the classical *mdx* strain of mice (19,20). We observed *Dock3* mRNA expression to be significantly elevated in the *mdx*^{5cv} muscles compared with aged-matched WT control muscles

across three different muscles types including the TA, soleus and diaphragm starting at 1 month of life (Fig. 1A–C). These findings of elevated *Dock3* mRNA were found to be consistent throughout adulthood into aged (12-month-old) *mdx*^{5cv} muscles (Fig. 1A–C).

Knockdown of dock3 mRNA in dystrophic zebrafish larvae improves muscle structure and overall outcomes

Zebrafish are a powerful model system for DMD disease modeling due to their translucent *ex vivo* development, large offspring sizes, ease of genetic manipulation and ability to uptake compounds in their skin and gills during early developmental stages (21–23). Zebrafish Dock3 protein amino acid sequences showed a strong amount of evolutionary conservation to mouse and human DOCK3 protein sequences (85% homology with mouse and human; Supplementary Material, Fig. S1). We performed *in situ* hybridization (ISH) for zebrafish *dock3* mRNA expression in WT (AB strain) zebrafish embryos at the early stages of development including prior to and after muscle formation. Zebrafish *dock3* mRNA was detected at low levels during early somite formation with strong expression in the developing brain, neural tube and dorsal muscle by 4 days post-fertilization (dpf) (Fig. 2A). The *sapje* zebrafish is a widely used DMD model that has the severe muscle weakness and myofiber degradation comparable to those observed in the later stages of DMD patient skeletal muscles (21,24,25). Unlike mammals, zebrafish lack definitive sex chromosomes and the *dystrophin* (*dmd*) gene in zebrafish is located on chromosome 1 (26). Mating of *sapje* heterozygote fish results in a Mendelian percentage of 25% affected zebrafish that can be easily identified via birefringence assay (24,25). The *sapje* homozygote mutant larvae showed severe myofiber disruption in affected larvae versus unaffected (*sapje* heterozygotes and WT) larvae (25,27–29) (Fig. 2B). Given our findings of increased *Dock3* expression in *mdx*^{5cv} muscles, we tested whether the modulation of zebrafish *dock3* expression might affect dystrophic outcomes. We observed significantly fewer than expected affected *sapje* zebrafish in our *dock3* morphant (*dock3* MO) zebrafish compared with control morphants when using a low dose of *dock3* morpholino (1 ng) (Fig. 2C). However, the high dose of *dock3* morpholino (6 ng) resulted in a higher number of affected *sapje* zebrafish, suggesting that there may be an optimal dose for blocking dystrophic pathology. These results were further confirmed using histochemical staining of F-actin in the dorsal muscles of the 1 ng *dock3* MO *sapje* zebrafish, which revealed fewer areas of myofiber detachment and overall more integrity compared with control MO *sapje* homozygotes, while the converse was observed for the high dose *dock3* morphant (Fig. 2D). Altogether, these data suggest that DOCK3 expression levels are strongly linked towards dystrophic pathologies and overall outcomes in DMD zebrafish.

Knockdown of DOCK3 in isolated human DMD myoblasts increases myogenic fusion

To investigate the effects of DOCK3 on myoblast fusion in dystrophin-deficient cells, we infected DMD and normal primary human myoblasts with lentiviral particles of either shRNA *DOCK3*, shRNA scrambled (i.e. non-targeting) or a mock control (Fig. 3A). DMD myoblasts have poor terminal differentiation into myotubes (30,31). We observed a significantly higher myogenic fusion index in the shRNAi *DOCK3* DMD myotubes compared with either shRNA scrambled or mock-treated DMD muscle cells (Fig. 3A and B). To validate the *DOCK3* mRNA knock-down, we performed western blot analysis for DOCK3 protein levels and confirmed a marked reduction of DOCK3 protein expression (Fig. 3C). These data reveal that the knockdown of *DOCK3* mRNA in human DMD myoblasts improves myogenic fusion percentages despite dystrophin-deficiency.

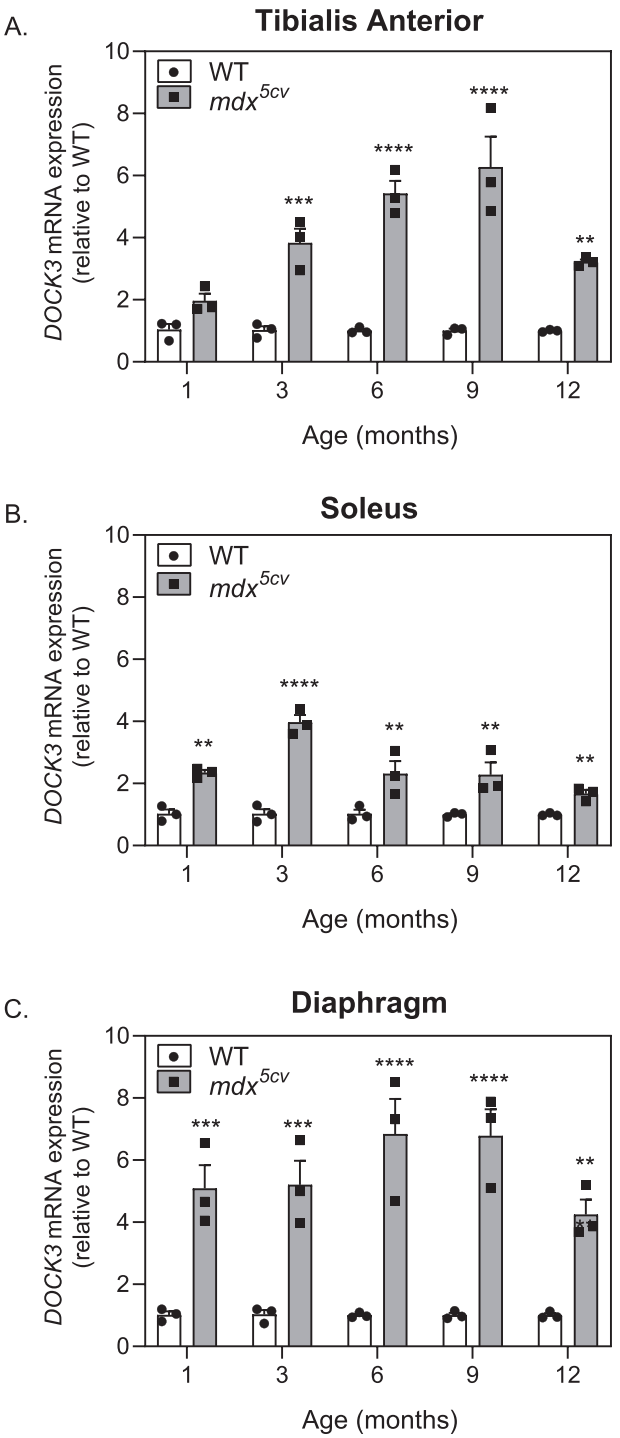

Figure 1. *Dock3* mRNA expression levels are increased in adult *mdx*^{5cv} mouse skeletal muscles. Real-time qPCR data from WT and *mdx*^{5cv} mice taken from (**A**) TA, (**B**) soleus and (**C**) diaphragm muscles at 1, 3, 6, 9 and 12 months of age demonstrating the significant increase in *Dock3* mRNA expression in *mdx*^{5cv} dystrophic mouse muscle compared with WT muscle ($n = 3$ per genotype and cohort, performed in triplicate; two-way ANOVA with Tukey's correction; $^{**}P < 0.01$, $^{***}P < 0.001$).

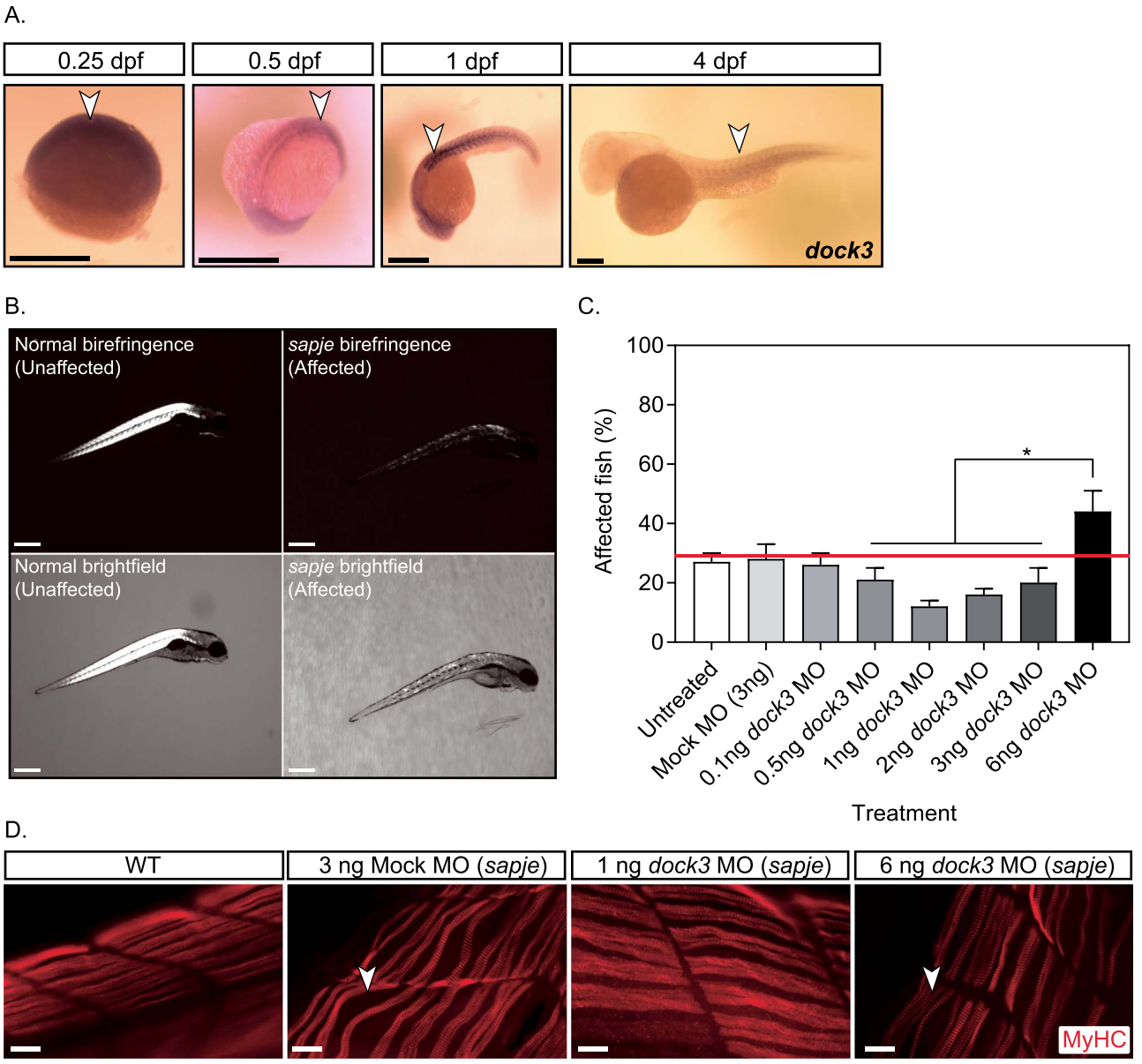

Figure 2. Knockdown of *dock3* mRNA in DMD zebrafish reduces dystrophic pathology. (**A**) ISH of zebrafish *dock3* mRNA during early developmental time points. Note the robust expression of zebrafish *dock3* mRNA in muscle tissues at stages of early muscle formation and muscle pioneer cell fusion. Not shown sense probes are used as internal controls. Arrowheads demarcate *dock3* mRNA ISH signal. Scale bar = 100 µm. (**B**) Representative images of normal and *sapje* mutant birefringence morphology. Scale bar = 200 µm. (**C**) Quantification of muscle birefringence shows that 1 ng of *dock3* MO improves muscle birefringence scoring in *sapje* mutant zebrafish, while 6 ng of *dock3* MO worsens muscle birefringence scoring. ($n = 3$ experimental replicates; one-way ANOVA with Tukey's correction; $^*P < 0.05$). (**D**) MyHC (F-59 antibody) immunofluorescent staining of 4 dpf WT (uninjected) or *sapje* mutant larvae injected with control (mock) morpholino, or *dock3* MO (1 or 6 ng). Arrowheads demarcate myofiber tears from the sarcolemmal membrane. Scale bar = 40 µm.

Knockdown of Dock3 in mdx^{5cv} mice improves cardiotoxin-induced muscle injury repair

We next investigated the role of DOCK3 in DMD pathology using the *mdx*^{5cv} mouse model of DMD. Given our findings of DOCK3 in myoblast fusion, we hypothesized that DOCK3 might play a role in muscle repair following injury. *Mdx*^{5cv} mice were co-injected with cardiotoxin (ctx) into the TA muscles along with either siRNA scrambled (control) or mouse *Dock3* siRNA (Fig. 3D). The *mdx*^{5cv} mice treated with *Dock3* siRNA had a more improved muscle injury repair pathology and muscle architecture compared with siRNA scrambled-treated mice 7 days after injury (Fig. 3E). The siRNA *Dock3*-treated *mdx*^{5cv} mice had significantly less centralized myonuclei than the control group (Fig. 3F). To validate *Dock3* mRNA knockdown, we performed western blot analysis which confirmed a strong reduction of DOCK3 protein expression levels (Fig. 3G). These results support a potential beneficial effect of reducing DOCK3 expression in the *mdx*^{5cv} mice during muscle injury-induced repair and regeneration.

Haploinsufficiency of *Dock3* improves muscle pathologies in *mdx*^{5cv} mice

Given our previous findings demonstrating that DOCK3 expression levels are elevated in DMD patients and *mdx*^{5cv} mice, we used *Dock3* global KO mice and evaluated their muscles on dystrophic *mdx*^{5cv} strain background in three separate cohorts.

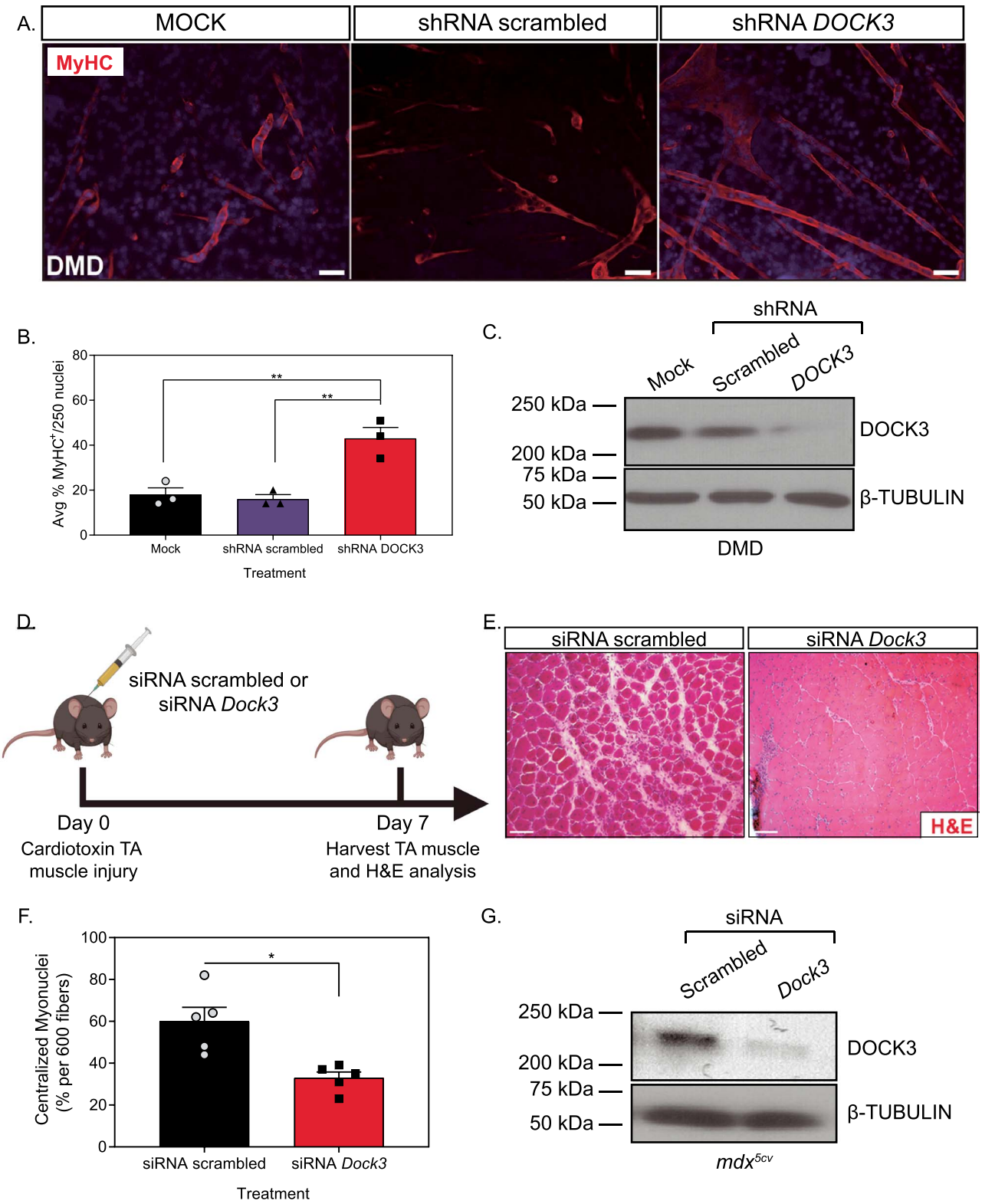

Figure 3. Knockdown of DOCK3 in DMD patient muscle cells and *mdx*^{5cv} mice increases myogenic differentiation and improves pathology. MyHC staining reveals that the knockdown of DOCK3 protein in human DMD primary myotubes increases myogenic fusion indices. (**A**) Immunofluorescence of MyHC (MF-20 antibody, DSHB Iowa, red) and nucleus marker (DAPI, blue) of Day 7 differentiated human DMD primary myotubes either transduced with mock (control), shRNA scrambled (negative control) and shRNA *DOCK3* lentiviral particles [transduced at a multiplicity of infection (MOI) of 10]. Scale bar = 50 μm. (**B**) Summary graph of average myogenic fusion indices as calculated by percentage of nuclei inside of MyHC^{+} cells out of 250 nuclei, as previously described (68). DMD primary myotubes transduced with shRNA *DOCK3* demonstrated significantly higher amount of myogenic fusion. ($n = 3$ experimental replicates, one-way ANOVA with Tukey's correction, $^{*}P < 0.05$). (**C**) Western blot analysis of whole cell lysates taken from Day 7 differentiated DMD myotubes transduced with mock (control), shRNA scrambled (shRNA internal control) or shRNA DOCK3 knockdown lentiviral particles, demonstrating successful knockdown of DOCK3 protein expression. (**D**) Schematic showing co-injection in *mdx*^{5cv} mice

Muscle architecture was assessed at 6 months of age across all groups by measuring a number of centralized myonuclei and fiber size distribution via hematoxylin and eosin (H&E) histochemistry (Fig. 4A–C), as well as measuring the severity of fibrosis via Masson's trichrome staining (Fig. 4D and E). Consistent with our initial findings, the global *Dock3* KO mice on *mdx*^{5cv} background [*Dock3*:*mdx*^{5cv} double KO (DKO)] mice developed exacerbated muscle weakness and all *Dock3*:*mdx*^{5cv} DKO mice expired by 6 months of age due to diaphragm muscle weakness (data not shown). Muscle structural analyses revealed severe myofiber disruption and fibrosis in the *Dock3*:*mdx*^{5cv} DKO mice compared with *mdx*^{5cv} (Fig. 4A–D). Interestingly, the haploinsufficiency of *Dock3* in *mdx*^{5cv} mice (*Dock3*$^{+/-}$:*mdx*^{5cv}) improved muscle fiber architecture, larger myofiber sizes and improved muscle pathology in comparison with the *mdx*^{5cv} and *Dock3*:*mdx*^{5cv} DKO double mutant mice (Fig. 4A–D). Western blot analysis revealed that *Dock3*$^{+/-}$:*mdx*^{5cv} mice had a 75% reduction in DOCK3 protein compared with *mdx*^{5cv} mice (Fig. 4F and G). These findings suggest that *Dock3* dosage levels influence the pathologic outcomes of dystrophin-deficient muscles and that the haploinsufficiency of *Dock3* is beneficial in dystrophic muscle pathology.

Adult Dock3 KO mice have abnormal muscle architecture, muscle mass and metabolism

Given our data demonstrating that the loss of DOCK3 expression in dystrophin-deficient muscle results in differential muscle effects, we further interrogated the role of DOCK3 expression in muscle health and metabolism in WT mice. Global *Dock3* KO mice had increased centralized myonuclei and altered fiber size distribution, indicating impaired muscle health compared with control WT mice (Fig. 5A–C). In addition, we observed significant muscle fiber atrophy reflected in smaller myofiber frequencies in the *Dock3* KO mouse muscle compared with control WT muscles (Fig. 5C). Additionally, adult *Dock3* KO mice had significantly lower body weight compared with WT mice at 6 months of age (Fig. 5D). Quantitative magnetic resonance (QMR) imaging in *Dock3* KO mice revealed reduced lean mass (Fig. 5E), while there was no effect on total fat mass (Fig. 5F) compared with WT mice. As muscle is the primary source of glucose and given our previous findings linking DOCK3 to the PTEN/AKT muscle growth pathway, we next measured the ability of *Dock3* KO mice to respond to a glucose challenge via a glucose tolerance test (GTT) (32). The GTT revealed that *Dock3* KO mice had a significantly impaired response to the glucose bolus, indicating a deficit in glucose metabolic processing (Fig. 5G). We then investigated the role of *Dock3* in global locomotor function using open field activity tracking to record basal activity levels in both aged-matched (6-month-old) WT and *Dock3* KO male mice. *Dock3* KO mice demonstrated significantly decreased distance traveled and average velocity compared with WT mice, indicating a reduction in basal locomotor function (Fig. 5H and I; Supplementary Material, Fig. S2). This demonstrates an decrease in locomotor ability in *Dock3* KO mice at 6 months of age similar to that reported for the *mdx* mouse model and consistent with our findings that *Dock3* KO mice have significant muscle weakness and myofiber atrophy (33–40). Additionally, we assessed cardiac function in WT and *Dock3* KO mice and found no significant differences in functional parameters (Supplementary Material, Fig. S3). These findings implicate a crucial role for DOCK3 in the maintenance of muscle mass and metabolic function in skeletal muscle.

RNA-sequencing of Dock3 KO muscles reveals dysregulated muscle transcripts

To determine what pathways may be affected by the loss of DOCK3 protein in muscle, we performed RNA-sequencing (RNA-seq) on adult TA skeletal muscles from WT and *Dock3* KO mice. Transcriptome analysis revealed 280 differentially expressed genes (DEGs) as shown by volcano plot (157 downregulated in blue and 123 upregulated in orange) (Fig. 6A). Gene ontology (GO) analyses revealed significant alterations in muscle structural and metabolic signaling pathways in the *Dock3* KO mice (Fig. 6B), which is consistent with the severe *Dock3* KO phenotype observed. We identified the top 10 up- and down-regulated transcripts, excluding undefined transcripts, of *Dock3* KO mice compared with WT by sorting top genes according to the statistical significance (adjusted *P*-value) and the strength of fold change induced ($\log_2$-fold change) (Fig. 6C and D). We confirmed a significant decrease in *Dock3* mRNA transcript in the *Dock3* KO mouse muscles (Fig. 6D). These findings reveal significant transcriptomic changes in important muscle structural and metabolic signaling pathways in the absence of DOCK3 protein.

Dock3 KO myoblasts fail to differentiate and have reduced myogenic fusion capabilities

Previous studies have demonstrated that DOCK1 and DOCK5 are essential for normal myoblast fusion and differentiation via actin nucleation factors (7,8,41). Additionally, previous studies have demonstrated that DOCK3 interacts with the WAVE complex to activate RAC1, modulate actin dynamics and promote cellular outgrowth (42). We postulated that DOCK3's function in modulating actin dynamics might influence muscle differentiation and fusion capabilities. We tested whether lentiviral shRNA knockdown of *DOCK3* mRNA affected myogenic differentiation capabilities in primary human muscle cells. Healthy human myoblasts were treated with either mock, shRNA scrambled (negative control) or shRNA *DOCK3* and assessed for myogenic differentiation capability using myosin heavy chain (MyHC) fluorescence (Fig. 7A). Myoblasts treated with shRNA *DOCK3* had significantly impaired myogenic differentiation compared with other control groups as evidenced by decreased amounts of MyHC-positive cells (Fig. 7B). Western blot analysis validated the reduction of DOCK3 protein levels by shRNA *DOCK3* mRNA knockdown (Fig. 7C). Moreover, we replicated this experiment using primary myoblasts isolated from our *Dock3* KO mice and WT mice and measured their myogenic differentiation capacity. We isolated primary myoblasts from adult WT and *Dock3* KO mouse TA muscles and evaluated their ability to fuse upon exposure to reduced serum medium. *Dock3* KO myoblasts showed poor myogenic differentiation capacity with an overall reduced amount of myotubes compared with aged-matched WT

of cardiotoxin (10 μM ctx) as well as either siRNA double-stranded (ds) oligos to inhibit mouse *Dock3* mRNA (siRNA *Dock3*) or a scrambled ds oligo (siRNA scrambled; control). Experiment was performed in each leg and mice were evaluated 7 days post ctx injury. (**E**) Representative H&E staining of the siRNA-injected *mdx*^{5cv} muscles 7 days post ctx. Scale bar = 50 μm. (**F**) Summary graph showing reduced centralized myonuclei when *mdx*^{5cv} mice were injected with siRNA *Dock3* ($n = 5$, student's *t*-test, two-tailed, $^{*}P < 0.05$). (**G**) Western blot analysis of whole muscle lysates from siRNA scrambled and siRNA *Dock3* muscle demonstrating successful knockdown of Dock3 protein.

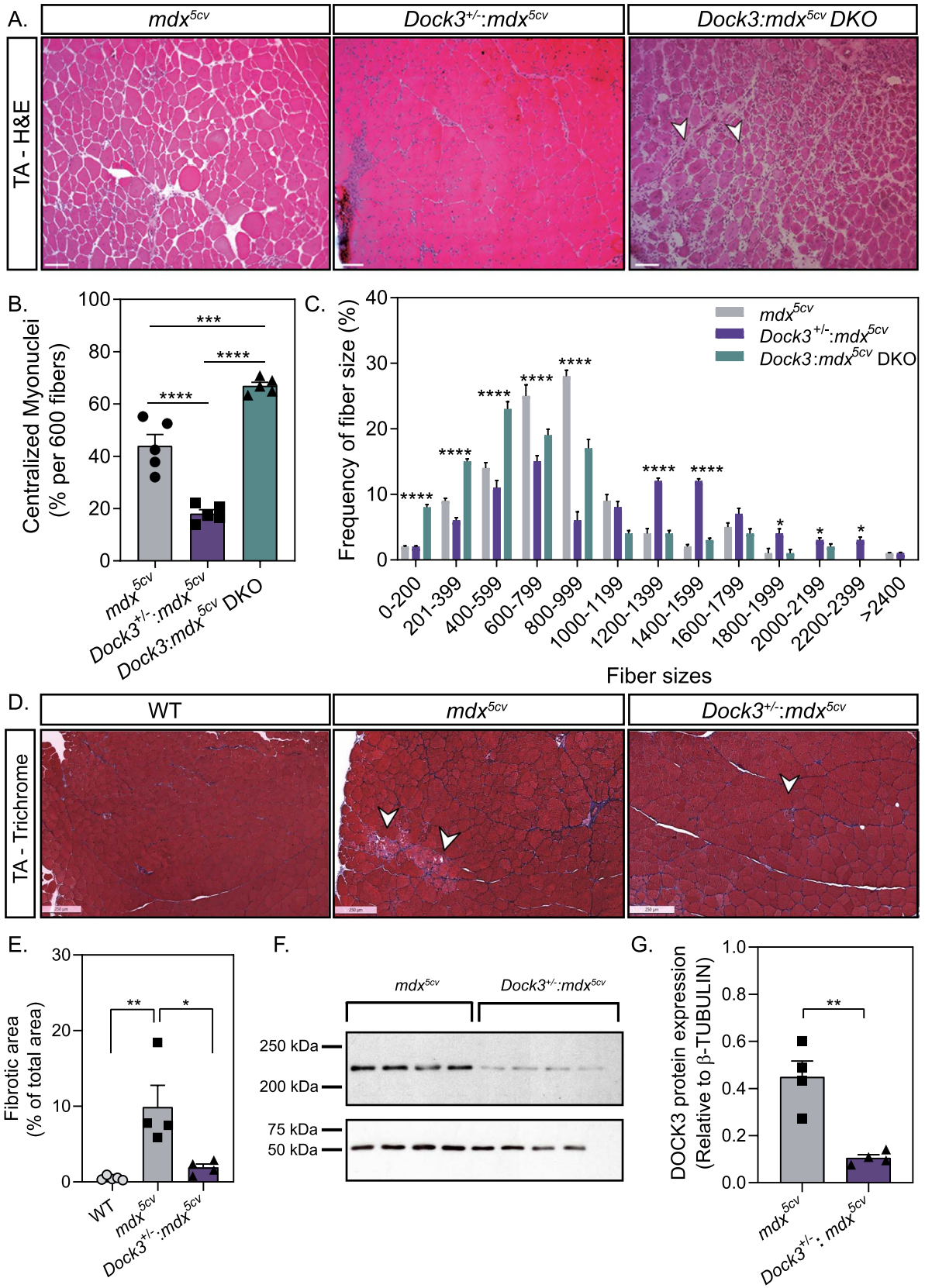

Figure 4. Gene dosage of *Dock3* affects muscle architecture and dystrophic pathology in mdx^{5cv} mice. (**A**) H&E immunohistochemistry of mdx^{5cv}, $Dock3^{+/-}$:mdx^{5cv} and *Dock3*:mdx^{5cv} DKO to visualize muscle morphology. Scale bar = 50 µm. Arrowheads indicate necrotic/fibrotic muscle. (**B**) Percent of centralized myonuclei out of 600 myofibers/TA comparing *Dock3* alleles on mdx^{5cv} genetic background. ($n = 5$, one-way ANOVA with Tukey's correction; $^{**}P < 0.01$, $^{****}P < 0.0001$). (**C**) Comparison of fiber size distribution curve based on CSA (µm^2) among *Dock3* alleles on mdx^{5cv} genetic background. ($n = 5$; two-way ANOVA with Tukey's correction; $^{*}P < 0.05$, $^{****}P < 0.0001$).

controls (Fig. 7D and E). Taken together, these studies demonstrate a critical role of DOCK3 protein in myogenic differentiation and myotube formation. As we noted a significant decrease in expression levels of the myogenic fusion peptide myomixer (*Mymx-Myomerger-Minion*) in *Dock3* KO TA muscles (Fig. 7D), we postulated that this decrease in myomixer-myomerger-minion expression may be the cause of the limited myogenic differentiation capacity of the *Dock3* KO myoblasts. We overexpressed FLAG-tagged *Mymx* (henceforth referred to as *Mymx* OE) or GFP in *Dock3* KO myoblasts. The *Dock3* KO myoblasts transfected with *Mymx-Myomerger-Minion* overexpression plasmid demonstrated a slightly increased percentage of multi-nucleated cells as observed by increase in the myogenic fusion index compared with the GFP-control (Supplementary Material, Fig. S4). Moreover, we found no significant difference in myogenic differentiation factors between *Mymx* OE and GFP *Dock3* KO myoblasts, indicating that overexpression of myomixer has minimal effects in improving the myogenic differentiation capability in the *Dock3* KO myoblasts in *Dock3* KO myoblasts (Supplementary Material, Fig. S4).

Discussion

We have identified *DOCK3* as a modifier of normal and dystrophin-deficient skeletal muscle health and function. First, we showed that DOCK3 is strongly elevated in expression levels in dystrophin-deficient mouse skeletal muscles consistent with the DOCK3 expression profile in human patients.[8] While complete loss of *Dock3* expression in *Dock3* KO and *Dock3:mdx*^{5cv} DKO mice have detrimental effects on skeletal muscles, haploinsufficiency of *Dock3*$^{+/-}$*:mdx*^{5cv} improves myofiber size and skeletal muscle pathology. These findings were further validated in the zebrafish *sapje* DMD zebrafish. Taken as a whole, these studies demonstrated that the reduction of *Dock3* expression in DMD models prevents the severity of dystrophic muscle pathology. These findings potentially represent the discovery of DOCK3 as new therapeutic target for DMD, as previous findings have identified factors that provide protective haploinsufficiency in *mdx* mice. For example, the haploinsufficiency of the transcription factors *Six4* and *Six5* in *mdx* mice similarly resulted in improved muscle grip strength and extended life span when haploinsufficient in *mdx* mice (43). While the roles of other DOCK proteins in muscle are not well described, it is possible that DOCK3 may have some overlapping and non-overlapping functions with DOCK4 based on similar protein sequence structure and domains. Studies in the *Dock4* KO mice revealed an essential role for DOCK4 in social behaviors and that the DOCK4-mediated activation of RAC1 in neurons could be overcome by constitutive RAC1 overexpression (44). Additional studies demonstrating that DOCK3 expression levels are tightly linked to RAC1 activation suggest that RAC1 activation may compensate for the loss of DOCK3 in muscle (45–47). Given our previous findings demonstrating that DOCK3 overexpression activates PTEN/AKT signaling in DMD muscle, the restoration of DOCK3 expression levels to that of WT muscle may restore RAC1 activation and could prevent the activation of cell death pathways that occurs in dystrophic muscles (14,48).

Complete loss of DOCK3 expression in both WT and dystrophin-deficient muscle resulted in worse muscle health, decreased myoblast fusion, glucose intolerance and defective muscle locomotive function. This is consistent with the reporting of clinical muscle hypotonia and muscle weakness in patients with pathogenic *DOCK3* variants (11–13). It is also consistent with the essential role of DOCK3 in axonal growth and the formation of protein aggregates leading to neurological deficits (10). Indeed, the compound loss of DOCK3 and the dystrophin protein likely impairs the myofiber membrane integrity and ability of RAC1 to be activated at the myofiber membrane. Thus, resulting in the exacerbated muscle pathologies that we observed in the *Dock3−/−:mdx5cv* double KO mice. Previous studies have demonstrated an essential role for dystrophin and an intact myofiber membrane to activate RAC1 (49,50). These studies are in compliment with ours and highlight an essential requirement for the dystrophin-associated protein complex as a requisite signaling hub for proper downstream signaling processes in skeletal muscle. The mechanism of action of DOCK3 in myogenesis and its role as a GEF remains of key interest to understand its function in muscle disease. As a GEF, DOCK3 activates RAC1, a Rho-GTPase, which has been shown to be tightly regulated in myogenesis (51). Overexpression of a constitutively active RAC1 in C_2C_{12} mouse skeletal myoblasts inhibits differentiation demonstrating the importance of RAC1 activation status in regulating temporal signals in myogenesis (52). Similar to the glucose impairment, we observed that in the *Dock3* KO mice, the muscle *Rac1* KO mice show impaired glucose processing (Raun *et al*., 2018). Interestingly, it has been shown that the overexpression of Def-6 (also called HMGB1), a GEF protein similar to DOCK3, impairs the downregulation of RAC1 activity and results in inhibited myogenic differentiation (53). These studies provide mechanistic insight into the molecular interplay between DOCK3 and RAC1 in dystrophin-deficient muscles and myogenesis.

Additionally, we observed multiple myogenic differentiation factors that were decreased in expression levels in the *Dock3* KO muscles via transcriptomic pathway analysis. A key question remains on whether DOCK3 functions to alter the filamentous actin in myoblasts or works through another mechanism to regulate the myogenic differentiation process. Our studies revealed that the overexpression of the myomixer-myomerger-minion peptide in *Dock3* KO myoblasts while slightly increasing the myogenic differentiation capability did not fully restore normal myogenic differentiation. It remains likely that DOCK3 has essential interactions with actin and other key molecules that may be the source of the impaired myogenic differentiation observed in the *Dock3* KO myoblasts.

Our findings provide evidence that DOCK3 plays a key role in normal muscle fusion and affects dystrophin-deficient muscle pathologies and outcomes. Furthermore, as DOCK3 expression levels are tightly correlated with dystrophic disease progression, DOCK3 may be a potential DMD biomarker that could be used to measure disease severity in muscle. Moreover, our findings also provide strong evidence for DOCK3 as a potential novel therapeutic target for the treatment of DMD. Future experiments aimed at further elucidating the mechanism of DOCK3 in muscle

(**D**) Masson's Trichrome stain to visualize fibrotic area in WT, *mdx*^{5cv} and *Dock3*$^{+/-}$*:mdx*^{5cv}. Scale bar = 250 µm. Arrowheads indicate fibrotic muscle. (**E**) Percent of fibrotic area comparing WT, *mdx*^{5cv} and *Dock3*$^{+/-}$*:mdx*^{5cv} TA muscle ($n = 4$, one-way ANOVA with Tukey's correction; $^{*}P < 0.05$, $^{**}P < 0.01$). (**F**) Western blot analysis of whole muscle lysate from *mdx*^{5cv} and *Dock3*$^{+/-}$*:mdx*^{5cv} mice for DOCK3 protein expression level quantification. (**G**) Quantification of DOCK3 protein expression level ($n = 4$, student's *t*-test, two-tailed, $^{**}P < 0.01$).

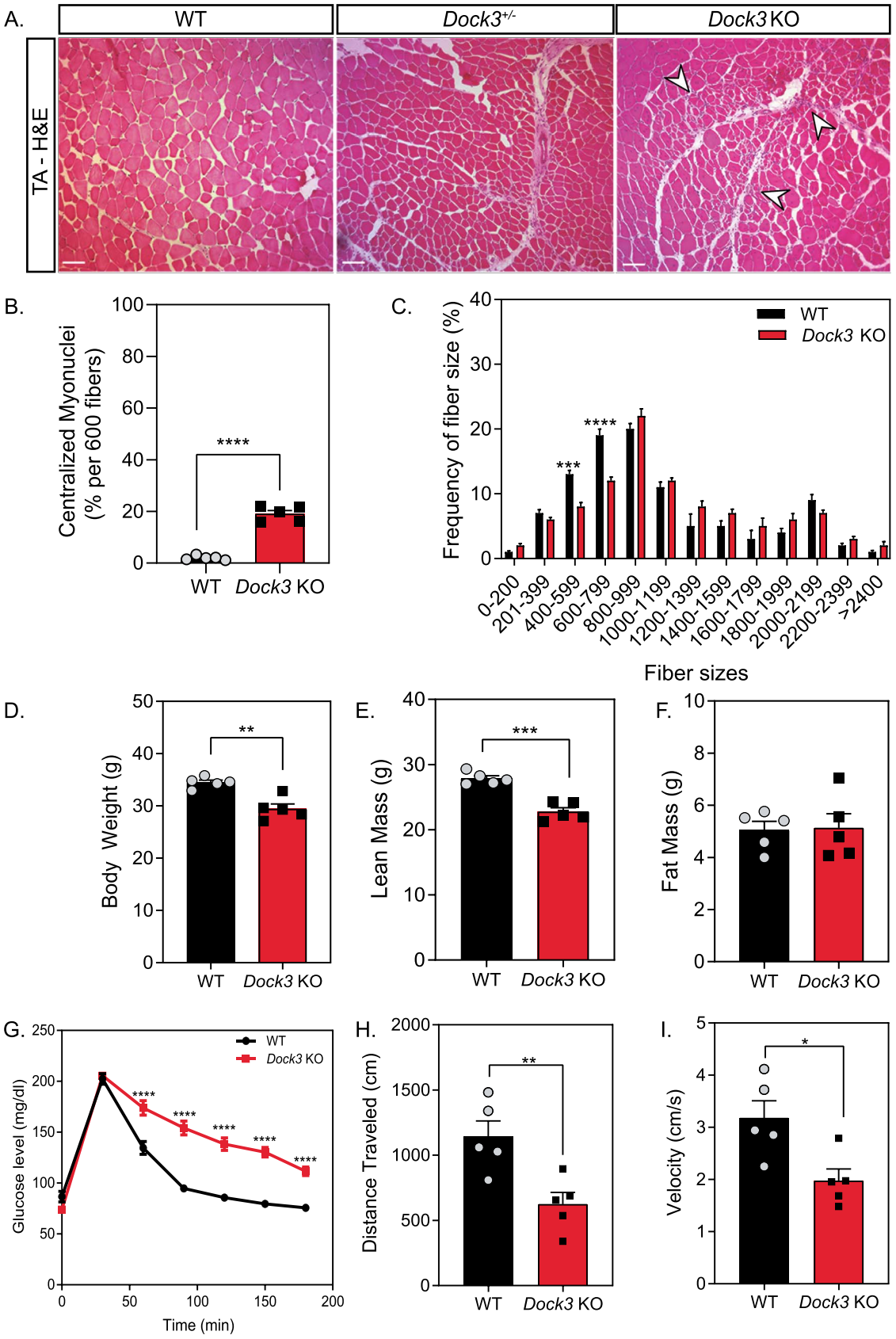

Figure 5. Adult *Dock3* KO mice have abnormal muscle architecture, muscle mass and metabolism. (**A**) H&E immunohistochemistry of *Dock3*$^{+/+}$ (WT), *Dock3*$^{+/-}$ and *Dock3* KO TA adult muscle on WT background. Scale bar = 50 µm. Arrowheads indicate necrotic/fibrotic muscle. (**B**) Percent of centralized myonuclei out of 600 myofibers/TA comparing WT and *Dock3* KO mice. ($n = 5$, student's *t*-test, two-tailed, $^{****}P < 0.0001$). (**C**) Comparison of WT and *Dock3* KO mice fiber size distribution curve based on

differentiation, signaling and its contribution towards muscle metabolic regulation are warranted.

Materials and Methods

Mice

Dock3 global KO mice (Jax mice stock# 033736) were obtained from the laboratory of Dr David Shubert (Salk Institute) and have been previously described (10). These mice contain a *beta-galactosidase* cassette integrated in-frame into exon 2 of mouse *Dock3* locus resulting in a complete disruption of the gene. WT (*C57BL/6 J*; stock# 000664) and mdx^{5cv} (stock# 002379) were originally obtained from Jackson Labs (Bar Harbor, ME). All mice were maintained on the *C57BL/6 J* strain background. All mouse strains were maintained under standard housing and feeding conditions with the University of Alabama at Birmingham Animal Resources Facility under pathogen-free, sterile conditions under the animal protocol number 21393.

Zebrafish morpholino experiments

WT *AB* and *sapje* (dmd^{ta222a} mutation on the *AB* strain background) zebrafish were used for all zebrafish morpholino experiments. A *dock3* morpholino (5′-GCCTCAGATCAATCAACTCGTTCAT-3′) and a control FITC-labeled (5′-CCTCTTACCTCAGTTACAATTTATA-3′) non-targeting morpholino (Gene Tools LLC; Philomath, OR) were used for all morpholino injections. Zebrafish morpholinos were injected into one-cell embryos obtained from *sapje* heterozygote matings at amounts of 0.1, 0.5, 1, 2, 3 and 6 nanograms (ng) in a solution of 1x Danieau buffer, water and phenol red (Sigma Aldrich, St. Louis, MO) as previously described (54). For MyHC zebrafish larvae were fixed in 4% paraformaldehyde (Electron Microscopy Sciences) overnight at 4°C and then following 3x washes in 1xPBS for 5 min were incubated for 1 h at room temperature with F-59 (MyHC; Developmental Studies Hybridoma Bank, Iowa City, IA) in the dark. Larvae were then washed 3x in 1xPBS for five min per wash and then incubated with anti-mouse Alexa Fluor-568 (Invitrogen; Cat# A-11004) for 45 min at room temperature in the dark. After an additional three washes in 1x PBS, the fish were then placed on superfrosted slides (FisherScientific; Waltham, MA) and imaged on a Nikon Eclipse E-1000 microscope. All adult fish were fed a standard diet of *Artemia salina* (brine shrimp) three times per day under a 14 h on, 10 h off light cycle in 3 L tanks with a density of no more than 20 fish per tank as standard of care guidelines. All zebrafish strains were maintained University of Alabama at Birmingham Animal Resources Aquatics Facility under pathogen-free conditions under the animal protocol number 20320.

Zebrafish muscle birefringence assay

Subsequently following the locomotor assay, birefringence assay was performed on 5 dpf larvae as previously described. Larvae were anesthetized using MS-222 and placed on microscope with polarizing light attachment. In this assay, when the polarized light is shone on the larvae, a white light is refracted back and captured in the camera if the muscle is healthy and has organized fibers. However, if the muscle is broken down and disorganized (worsened muscle phenotype), the polarized light will shine straight through and will appear in the camera as black (absence of white refracted light).

ISH zebrafish experiments

The zebrafish *dock3* mRNA (*dock3–201* ENSEMBLE transcript; ENSDARG00000063180) was used as a template and an antisense region containing 300 base pairs sequence of the end of *dock3* mRNA coding sequence was used for *in vitro* transcription probe synthesis. *In vitro* transcription reactions performed using the MegaScript Sp6 (Cat# AM 1330) and MegaScript T7 Transcription (Cat# AM 1334) kits (ThermoFisher Scientific) were used following the manufacturer's guidelines. Morpholino injected zebrafish embryos were placed in fish water containing 1x PTU (Sigma; Cat# P7629) at 24 h post-fertilization. ISH reactions were performed on 4% paraformaldehyde (Electron Microscopy Sciences; Hatfield, PA; Cat# 15710) zebrafish embryos using the DIG RNA Labeling Kit (MilliporeSigma; Burlington, MA; Cat# 11175025910) following a standardized protocol (55). The DIG-labeled embryos were imaged under the dissection scope (Nikon, SMZ1500; Tokyo, Japan) with EXFO Fluorescence illumination system, X-Cite 120 (Photonic Solutions Inc.; Edinburgh, UK), using a Nikon Eclipse E-1000 microscope attached to a Hamamatsu digital camera, and images were acquired using Openlab software version 3.1.5 (Improvision; PerkinElmer; Waltham, MA).

Human muscle samples

Primary vastus lateralis muscle biopsies from normal and DMD patients were obtained from consented patients under the approved Boston Children's Hospital protocol 03-12-205 and described elsewhere (14,15). Additional samples were collected under the UAB protocol 300 002 164. All patient samples were de-identified and the secondary confirmation of DMD mutations was performed using MLPA analysis and/or exome sequencing (56).

Mouse activity tracking

Mouse locomotive activity measurements were performed as previously described (57). Twenty-four hours prior to experiment termination and tissue harvest, mice were analyzed for locomotive activity using the Ethovision XT software platform (Noldus; Leesburg, VA) with isolated individual chambers adapted from a previously described protocol (14). Mice were adapted to the room and open-field chambers 1 day prior to activity and were given a 5-min additional adaptation period prior to activity recording. Mouse activity was recorded for 6 min with no external stimulation.

Myofiber and myogenic fusion calculations

The cross-sectional area (CSA) of the skeletal muscle sections was calculated in a manner previously described (14). Briefly, 600 TA myofibers were counted and CSA (μm^2) was measured via a series of overlapping H&E microscopy images, and quantified in

CSA (μm^2). ($n = 5$; two-way ANOVA with Tukey's correction; $^{***}P < 0.001$, $^{****}P < 0.0001$). (**D**) Compared with WT mice, *Dock3* KO mice were significantly lower in gross body weight, (**E**) had significantly decreased lean mass and (**F**) had no difference in fat mass observed. ($n = 5$; student's *t*-test, two-tailed; $^{**}P < 0.01$, $^{***}P < 0.001$). (**G**) GTT revealed that *Dock3* KO mice are glucose intolerant. ($n = 5$; two-way ANOVA with Tukey's correction; $^{****}P < 0.0001$). (**H**) *Dock3* KO mice had significantly decreased distance traveled ($n = 5$; student's *t*-test, two-tailed; $^{**}P < 0.01$). (**I**) *Dock3* KO mice had significantly decreased average velocity ($n = 5$; student's *t*-test, two-tailed; $^{*}P < 0.05$).

A.

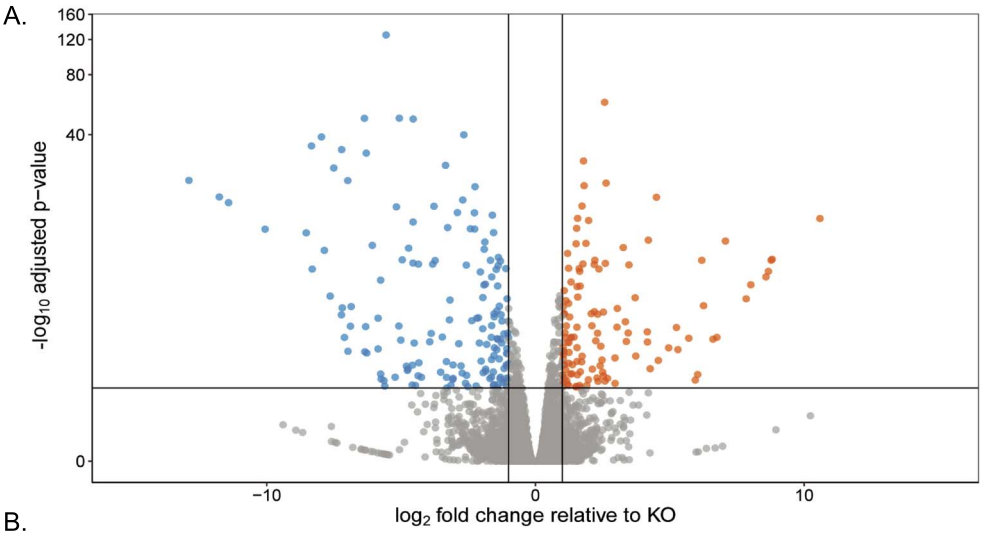

B.

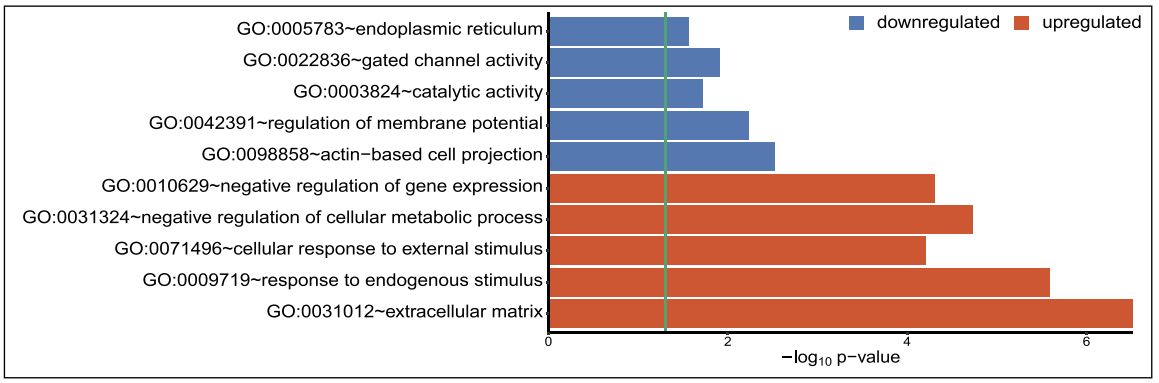

C.

	Gene Symbol	Gene Description	Log_2 Fold Change (KO vs WT)	Adjusted p-value
1	Hist1h4m	histone cluster 1, H4m	10.59	1.62E-15
2	Kpna2	karyopherin (importin) alpha 2	4.50	7.86E-20
3	Rab6b	RAB6B, member RAS oncogene family	3.45	5.04E-04
4	Mib1	mindbomb E3 ubiquitin protein ligase 1	2.57	5.94E-59
5	Pdk4	pyruvate dehydrogenase kinase, isoenzyme 4	2.41	1.09E-02
6	Angptl4	angiopoietin-like 4	2.33	3.31E-02
7	Fbxo44	F-box protein 44	2.19	3.34E-05
8	Fosb	FBJ osteosarcoma oncogene B	2.12	1.42E-02
9	Ang	angiogenin, ribonuclease, RNase A family, 5	2.10	2.17E-04
10	Ucp3	uncoupling protein 3 (mitochondrial, proton carrier)	1.91	4.28E-02

D.

	Gene Symbol	Gene Description	Log_2 Fold Change (KO vs WT)	Adjusted p-value
1	Rpl3-ps1	ribosomal protein L3, pseudogene 1	-11.42	1.20E-18
2	Mymx	myomixer, myomerger, minion, myoblast fusion factor	-6.88	2.28E-04
3	Clca1	chloride channel accessory 1	-5.74	2.85E-02
4	Gdf5	growth differentiation factor 5	-5.22	2.52E-02
5	Cdk6	cyclin-dependent kinase 6	-5.06	3.86E-49
6	Gabrb3	gamma-aminobutyric acid (GABA) A receptor, subunit beta 3	-4.37	2.28E-02
7	Dock3	dedicator of cyto-kinesis 3	-4.34	8.63E-03
8	Cacna1i	calcium channel, voltage-dependent, alpha 1I subunit	-3.53	1.77E-02
9	Sln	sarcolipin	-2.90	1.29E-16
10	Rrad	Ras-related associated with diabetes	-2.18	8.18E-05

Figure 6. RNA-sequencing analysis of *Dock3* KO TA muscles reveals numerous dysregulated mRNA transcripts and signaling pathways. (**A**) Summary graph of differentially regulated genes, with blue representing downregulated genes and orange representing upregulated genes relative to KO. (**B**) Top downregulated and upregulated GO terms as determined by GO analyses compared with WT. (**C**) Top 10 upregulated genes in *Dock3* KO mice compared with WT. (**D**) Top 10 downregulated genes in *Dock3* KO mice compared with WT. Highlighted in blue are specific genes of interest.

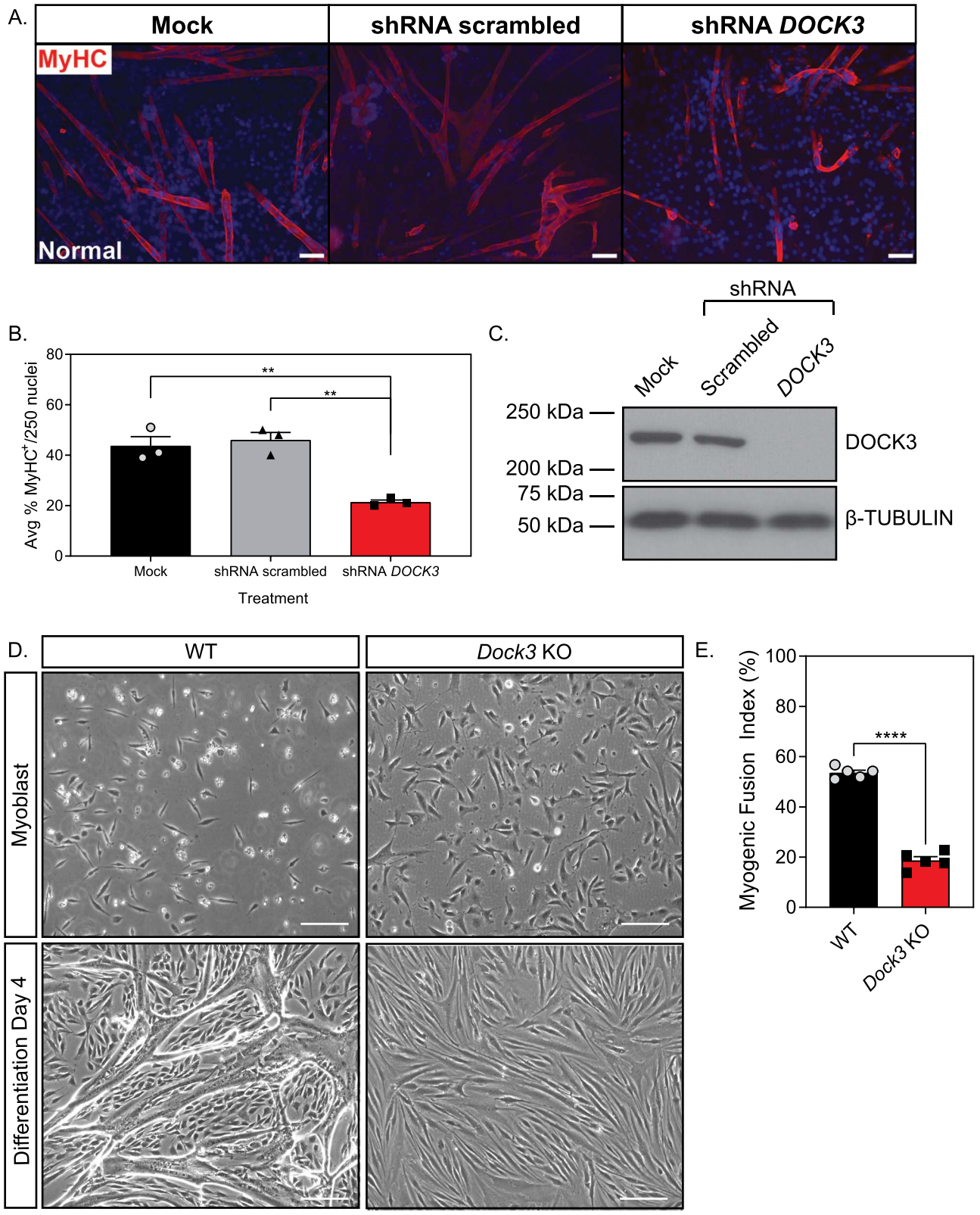

Figure 7. DOCK3 is essential for normal myoblast fusion. (**A**) MyHC staining reveals that knockdown of DOCK3 protein in normal human primary myotubes decreases myogenic fusion indices. MyHC (MF-20 antibody, DSHB Iowa, red) immunofluorescence of Day 7 differentiated primary myotubes along with DAPI (blue). MOCK, shRNA scrambled and shRNA *DOCK3* lentiviral particles were transduced at an MOI of 10. Scale bar = 50 µm. (**B**) Average myogenic fusion indices as calculated by percentage of nuclei inside of MyHC^{+} cells out of 250 nuclei as previously described (68). Myotubes with shRNA *DOCK3* knockdown have significantly less myogenic fusion than shRNA scrambled control ($n = 3$ experimental replicates; one-way ANOVA with Tukey's correction; $^{*}P < 0.05$). (**C**) Western blot analysis of whole cell lysates taken from normal human Day 7 differentiated myotubes transduced with mock (control), scrambled (shRNA internal control) or shRNA *DOCK3* knockdown inhibitor lentiviral particles showing successful knockdown of DOCK3 protein expression. (**D**) Representative images of WT and *Dock3* KO mouse myoblasts undergoing differentiation. (**E**) Quantification of myogenic fusion index where *Dock3* KO mouse myoblasts has significantly less myogenic fusion than WT mouse myoblasts. Scale bar = 100 µm. ($n = 5$; student's *t*-test, two-tailed; $^{****}P < 0.0001$).

Fiji software platform (58). Myogenic fusion indices were determined by immunofluorescent staining using the MF-20 (MyHC) as a marker of myogenic differentiation. Fusion of myoblasts was determined by the detection of more than one nuclei within an MyHC+ myotube.

DEXA QMR imaging

To evaluate body composition (fat and lean tissue mass) *in vivo*, 6-month male WT and *Dock3* KO mice (5 mice/genotype) were measured using the EchoMRI™ 3-in-1 composition analyzer (software version 2016, Echo Medical, Houston, TX). Individual fat and lean mass measurements were measured in grams (g) and were analyzed using student's *t*-test between WT and *Dock3* KO mice.

Glucose tolerance test

Mice were fasted for 16 h prior to afternoon administration of a bolus of D-glucose (MilliporeSigma; Cat# G8270) which was intraperitoneal injected at a concentration of 3 mg/gram of mouse body weight. Blood glucose was measured on a commercially obtained glucometer (Nipro Diagnostics; Ft. Lauderdale, FL) using 10 µL of whole serum from tail bleeds placed on standardized glucose meter test strips.

siRNA knockdown in cardiotoxin-injured muscles

Adult male *mdx*^{5cv} mice (4–6 months old) were injected in their TA skeletal muscles with cardiotoxin (10 µM) and siRNA pooled oligos (10 µg; GE Healthcare Dharmacon Inc; Lafayette, CO) containing either scrambled siRNAs or siRNAs targeting mouse *Dock3* mRNA following a protocol previously established (59). The contralateral TA muscle was used as a sham phosphate-buffered saline (ThermoFisher Scientific; Waltham, MA; Cat#10010049) control. Seven days following injections, mice were euthanized, and their TA skeletal muscles were slow-frozen in TissuePlus O.C.T (FisherScientific; Hampton, NH; Cat#23–730-571), for histological and molecular analysis.

Immunofluorescence and immunohistochemistry

Mouse skeletal muscles were cryo-frozen in a TissuePlus O.C.T (FisherScientific; Hampton, NH; Cat#23–730-571) Isopentane (FisherScientific; Cat# AC397221000) liquid nitrogen bath as unfixed tissues. Mouse hearts were perfusion fixed in 10% neutral buffered formalin (MilliporeSigma) overnight at 4°C, which was performed before embedding the tissue sample into paraffin blocks. Blocks were later cut on a cryostat and 7- to 10-µm-thick sections were placed on SuperFrost Plus Gold slides (ThermoFisher; Cat# FT4981GLPLUS). H&E staining was performed as previously described (15). For immunofluorescent staining, following de-paraffinization, the slides were incubated in eBioscience IHC Antigen Retrieval Solution (ThermoFisher; Cat# 00–4955-58) and washed in 1x PBS three times for 5 min, and then incubated with blocking reagent from the Mouse-on-Mouse (M.O.M) kit (Vector Laboratories; Burlingame, CA; Cat# BMK-2202). Slides were incubated for 1 h at room temperature in primary antibody.

Western blot

Protein lysates were obtained from either pestle-homogenized tissues or cell lysates in M-PER lysis buffer (ThermoFisher; Cat# 78501) supplemented with 1x Complete Mini EDTA-Free protease inhibitor cocktail tablets (Roche Applied Sciences; Cat# 04693159001; Penzburg, Germany). Protein lysates were quantified using a Pierce BCA Protein Assay Kit (ThermoFisher; Cat# 23225). Unless stated otherwise, 50 µg of whole protein lysate was used for all immunoblots, and electrophoretically resolved on 4–20% Novex tris-glycine gels (ThermoFisher: Cat# XPO4205BOX). Protein samples were then transferred to 0.2 µm PVDF membranes (ThermoFisher: Cat# LC2002), blocked in 0.1x TBS-Tween in 5% non-fat milk for 1 h before being incubated in primary antibody overnight at 4°C with gentle rocking. Blots were washed in 0.1% TBS-Tween three times for 5-min intervals before being incubated with secondary antisera (mouse or rabbit) conjugated to horse radish peroxidase (HRP) for 1 h at room temperature with gentle agitation. Membranes were then washed in 0.1% TBS-Tween three times for 5-min intervals before being incubated with secondary antibodies (either mouse or rabbit) conjugated to HRP for 1 h at room temperature with gentle agitation. Following another three washes for 15-min intervals at room temperature, membranes were then treated with RapidStep ECL Reagent (MilliporeSigma; Cat# 345818-100ML) and exposed to X-ray film (Genesee Scientific). Some Western blot images were acquired using a Typhoon Variable Mode Imager (Amersham Pharmacia; Little Chalfont, UK). Some membranes were stripped using Restore Plus Western Blot Stripping Buffer (ThermoScientific; Cat# 46428) and later probed with a different primary antibody.

RNA-sequencing and data analyses

Adult male 6-month-old WT and *Dock3* KO mouse TA muscles ($n = 3$ muscles per genotype cohort) were biopsied, and total RNA was extracted following mechanical homogenization using the GenElute Total RNA Purification Kit (MilliporeSigma; Cat# RNB100-50RXN) following the manufacturer's guidelines. The total RNA was amplified using the Sure Select Stranded RNA-Seq kit (Agilent Technologies; Santa Clara, CA) using standard protocols. A ribominus kit (ThermoFisher; Cat# K155002) was used to deplete large ribosomal RNAs. The sequencing was done on the Illumina HiSeq2500 in paired-end mode following the manufacturer's protocols by the UAB Genomics Core Facility.

All biological replicates contained a minimum of 35.7 million reads with an average number of 39.6 million reads across the replicates. The FASTQ files were uploaded to the UAB high-performance computer cluster for bioinformatics analysis with the following custom pipeline built in the Snakemake workflow system (v5.2.2) (60): first, quality and control of the reads were assessed using FastQC, and trimming of the Illumina adapters and bases with quality scores of less than 20 were performed with Trim_Galore! (v0.4.5). Following trimming, the transcripts were quasi-mapped and quantified with Salmon (61) (v0.12.0, with '—gencode' flag for index generation and '-l ISR', '—gcBias' and '—validateMappings' flags for quasi-mapping) to the mm10 mouse transcriptome from Gencode release 21. The average quasi-mapping rate was 70.4% and the logs of reports were summarized and visualized using MultiQC (62) (v1.6). The quantification results were imported into a local RStudio session (R version 3.5.3) and the package 'tximport' (63) (v1.10.0) was utilized for gene-level summarization. Differential expression analysis was conducted with DESeq2 (64) package (v1.22.1). Following count normalization, principal component analysis was performed and genes were defined as DEGs if they passed a statistical cutoff containing an adjusted *P*-value <0.05 (Benjamini–Hochberg false

discovery rate method) and if they contained an absolute $\log_2$-fold change ≥ 1. Functional annotation enrichment analysis was performed in the NIH Database for Annotation, Visualization and Integrated Discovery (DAVID, v6.8) by separately submitting upregulated and downregulated DEGs. A *P*-value <0.05 cutoff was applied to identify GO terms.

The FASTQ files of the current study have been uploaded to NCBI's Gene Expression Omnibus under accession number GSE141621.

Real-time quantitative PCR

Total RNA was extracted using the miRVana (ThermoFisher; Cat# AM1560) kit following the manufacturer's protocol. One microgram of total RNA was reverse transcribed using the Taqman Reverse Transcription kit following the manufacturer's protocol (Applied Biosystems; Foster City, CA; Cat# N8080234). Taqman assay probes were all purchased from Applied Biosystems corresponding to each individual gene. Quantitative PCR (qPCR) Taqman reactions were performed using Taqman Universal PCR Master Mix (Applied Biosystems; Cat# 4304437). Samples were run on the Fluidigm Biomark HD platform (Fluidigm Corp.; San Francisco, CA) in 96.96 dynamic array plates. Relative expression values were calculated using the manufacturer's software and further confirmed using the $2^{-\Delta\Delta Ct}$ method (65).

Muscle myoblast cell cultures

Primary muscle cells were isolated from postnatal 7-day-old WT or *Dock3* KO mouse hindlimbs via a pre-plate purification strategy for enrichment of a slow-adhering purification as previously described (66,67). Primary muscle cells were later evaluated for myogenic capacity via immunofluorescent staining of desmin to ensure for a myogenic population greater than 95%. Muscle cells were grown in skeletal muscle growth medium (Promocell; Heidelberg, Germany; Cat# C-23060) supplemented with 1x antibiotic-antimycotic (ThermoFisher Scientific; Cat# 15240062) and 1 ng/10 mL rhFGF (Promega; Madison, WI; Cat# G5071). Cells were seeded at a density of 1.5×10^6 per 10 cm^2 plate or 2-chamber slides (Corning Inc.; Corning, NY) coated with 1% rat tail collagen (Millipore Sigma; Cat# 08–115). When cells reached 90% confluency, they were switched to differentiation medium, which is composed of DMEM GlutaMAX™, 1% of Antibiotic-Anti-mycotic (Invitrogen: Cat# 1520) and Promocell Human Skeletal Muscle Differentiation Media (Cat# C-23061). Myogenic fusion assays and immunofluorescent labeling were performed as previously described (68).

Nucleofection of myomixer fusion protein in mouse Dock3 KO primary myoblasts

Myomixer-FLAG was packaged in the pLVX-TetON (Takara Bio; Mountain View, CA) plasmid and have been described in previous literature (69). The plasmid was subcloned into pIRES-1a-hrGFP (Stratagene; San Diego, CA) plasmid. Nucleofection of *Dock3* KO primary myoblasts in culture was done according to the optimized protocol for skeletal muscle myoblasts following the manufacturer's protocol (Lonza; Basel, Switzerland). Briefly, myoblasts were grown in their respective culture media in 100 cm^2 plates until they reached 80% confluency, corresponding to approximately 1.5 x 10^6 cells. The medium was removed from the plate and cells were trypsinized with 1 mL of trypsin–EDTA (Invitrogen) to detach them completely. Subsequently, 4 mL of medium was added to the plate and then the cells and the culture medium were centrifuged at 1000× g for 5 min at room temperature. The supernatant was then removed, and cell pellets were resuspended in 100 µL of Nucleofector solution (Lonza) in which either 2 ug of myomixer plasmid or 2 ug pmaxGFP plasmid were added to respective cohorts. The cells were analyzed 24–48 h after the nucleofection by fluorescence microscopy with an inverted Leica microscope. After 48 h post-nucleofection, proliferation media was removed and washed with 1× PBS (Dulbecco) which was aspirated and replaced with differentiation media.

Myogenic fusion assays

Myoblasts from *Dock3* global KO mice were nucleofected with myomixer-FLAG and its GFP control in four-well chamber slides at 100 000 cells/per well, separately (as described above). To assess myogenic fusion, cells were fixed at day 4 of differentiation with 4% paraformaldehyde for 20 min at 4°C followed by permeabilization with 0.1% triton™X-100 (Sigma Aldrich) for 30 min at room temperature and blocking in 1xPBS with 1% fetal bovine serum (Gibco). Cells were incubated with primary antibody for MyHC (MF-20—1:100, Developmental Studies Hybridoma Bank) overnight at 4°C, followed by three washes with 1x PBS and incubation with secondary antibody Alexa Fluor 555 (Invitrogen). Slides were washed and mounted with Vectashield® Mounting Media (Vector) with DAPI. Images were obtained in Zeiss 710 confocal system at 20X. The fusion index was calculated as follows: (MF20-stained myocytes containing ≥ 2 nuclei/total number of nuclei) $\times$ 100, as previously described (70).

CLUSTAL Omega alignment

CLUSTAL Omega alignments using freely available software (https://www.ebi.ac.uk/Tools/msa/clustalo/) as described (71). Accession numbers for protein sequences: zebrafish (*Danio rerio*, XP_009294754.1), mouse (*Mus musculus*, NP_700462.2) and human (*Homo sapiens*, NP_004938.1).

Cardiac functional measurements: transthoracic echocardiography

The Vevo 3100 (VisualSonics Inc, Canada) imaging system was used for echocardiography to evaluate individual parameters of cardiac structure and function *in vivo*. Six-month male WT and *Dock3* KO mice (5 mice/genotype) were anesthetized using 1–2% isofluorane continuously suppled from surgivet vaporizer, and both long- and short-axis high-resolution images were acquired for heart function measurements and analysis. Each individual parametric measurement was compared between WT and *Dock3* KO mice using a student's *t*-test (Supplementary Material, Fig. S3).

Statistical analyses

All graphs were represented as mean ± SEM. Unless otherwise mentioned, a two-tailed student's *t*-test was performed for all single comparisons and either a one-way or two-way analysis of variance (ANOVA) with Tukey correction was performed for all multiple comparisons. GraphPad Prism version 8 software (GraphPad Software; San Diego, CA) was used for all statistical analyses. An *a priori* hypothesis of $^*P < 0.05$, $^{**}P < 0.01$, $^{***}P < 0.001$ and $^{****}P < 0.0001$ was used for all data analysis.

Supplementary Material

Supplementary Material is available at *HMG* online.

Acknowledgements

We would like to thank Dr David Schubert (Salk Institute) for the generous gift of the *Dock3* KO mice. We would like to thank Dr Michael Crowley and the staff of the UAB Genomics Core Facility for RNA-sequencing processing and initial analyses. We would like to thank Eddie Bradley for the mouse cardiovascular function analyses. We would like to thank Drs Timothy Nagy and Maria Johnson at the UAB Small Animal Phenotyping Core for DEXA measurements. We would like to thank Drs David Schneider (UAB), Glenn Rowe (UAB) and Emanuela Gussoni (Boston Children's Hospital) for critical reading of our manuscript. We would like to thank Dr Susan Farmer and her staff for care and maintenance of our animals. Lastly, we would like to thank the patients and their families who contributed samples that were used in this study and helped to make this research possible.

Conflict of Interest statement. All authors declare no conflicts of interest.

Funding

R.M.H. is a member of the NIH-supported RoadMap Scholars Program grant and is also supported by a training fellowship sponsored by the University of Alabama at Birmingham Center for Exercise Medicine grant number T32HD071866. R.M.H. is a funded by an NIH National Institute of Neurological Disorders and Stroke (NINDS) F99/K00 grant (F99NS118718). The UAB Small Animal Phenotyping Core supported by the NIH Nutrition & Obesity Research Center (P30DK056336) and the Mouse Cardiovascular Core Vevo 3100 Mouse Ultrasound Facility for this project. Research reported in this publication was supported by the Eunice Kennedy Shriver National Institute of Child Health and Human Development, NIH and HHS of the National Institutes of Health under award number R01HD095897 awarded to M.S.A. M.S.A. is also a co-investigator on an NIH NIAMS award R21AR074006. M.S.A. is funded by a Muscular Dystrophy Association grant (MDA41854). UAB Small Animal Phenotyping Core supported by the NIH Nutrition & Obesity Research Center P30DK056336, Diabetes Research Center P30DK079626 and the UAB Nathan Shock Center P30AG050886A. T.V.G. is funded by NIH P30NS47466. L.J. D. is funded by NIH grant P01HL051952 and the Department of Veterans Grant 1CX000993-01. G.V.H. is funded by NIH R01 grants HL132989 and HL144788. D.P.M. is funded by NIH grants R01 grants AR068286 and AG059605.

References

1. Ballarino, M., Morlando, M., Fatica, A. and Bozzoni, I. (2016) Non-coding RNAs in muscle differentiation and musculoskeletal disease. *J. Clin. Invest.*, **126**, 2021–2030.
2. Cacchiarelli, D., Incitti, T., Martone, J., Cesana, M., Cazzella, V., Santini, T., Sthandier, O. and Bozzoni, I. (2011) miR-31 modulates dystrophin expression: new implications for Duchenne muscular dystrophy therapy. *EMBO Rep.*, **12**, 136–141.
3. Waldrop, M.A., Gumienny, F., El Husayni, S., Frank, D.E., Weiss, R.B. and Flanigan, K.M. (2018) Low-level dystrophin expression attenuating the dystrophinopathy phenotype. *Neuromuscul Disord*, **28**, 116–121.
4. Peter, A.K. and Crosbie, R.H. (2006) Hypertrophic response of Duchenne and limb-girdle muscular dystrophies is associated with activation of Akt pathway. *Exp. Cell Res.*, **312**, 2580–2591.
5. Dumont, N.A., Wang, Y.X., von Maltzahn, J., Pasut, A., Bentzinger, C.F., Brun, C.E. and Rudnicki, M.A. (2015) Dystrophin expression in muscle stem cells regulates their polarity and asymmetric division. *Nat. Med.*, **21**, 1455–1463.
6. Laurin, M. and Côté, J.-F. (2014) Insights into the biological functions of Dock family guanine nucleotide exchange factors. *Genes Dev.*, **28**, 533–547.
7. Moore, C.A., Parkin, C.A., Bidet, Y. and Ingham, P.W. (2007) A role for the myoblast city homologues Dock1 and Dock5 and the adaptor proteins Crk and Crk-like in zebrafish myoblast fusion. *Development*, **134**, 3145–3153.
8. Laurin, M., Fradet, N., Blangy, A., Hall, A., Vuori, K. and Côté, J.-F. (2008) The atypical Rac activator Dock180 (Dock1) regulates myoblast fusion in vivo. *Proc. Natl. Acad. Sci.*, **105**, 15446–15451.
9. Makihara, S., Morin, S., Ferent, J., Côté, J.-F., Yam, P.T. and Charron, F. (2018) Polarized Dock activity drives Shh-mediated axon guidance. *Dev. Cell*, **46**, 410–425.e417.
10. Chen, Q., Peto, C.A., Shelton, G.D., Mizisin, A., Sawchenko, P.E. and Schubert, D. (2009) Loss of modifier of cell adhesion reveals a pathway leading to axonal degeneration. *J. Neurosci.*, **29**, 118–130.
11. Helbig, K.L., Mroske, C., Moorthy, D., Sajan, S.A. and Velinov, M. (2017) Biallelic loss-of-function variants in DOCK3 cause muscle hypotonia, ataxia, and intellectual disability. *Clin. Genet.*, **92**, 430–433. doi: 10.1111/cge.12995.
12. Iwata-Otsubo, A., Ritter, A.L., Weckselbatt, B., Ryan, N.R., Burgess, D., Conlin, L.K. and Izumi, K. (2018) DOCK3-related neurodevelopmental syndrome: Biallelic intragenic deletion of DOCK3 in a boy with developmental delay and hypotonia. *Am. J. Med. Genet. A*, **176**, 241–245.
13. Wiltrout, K., Ferrer, A., van de Laar, I., Namekata, K., Harada, T., Klee, E.W., Zimmerman, M.T., Cousin, M.A., Kempainen, J.L., Babovic-Vuksanovic, D. *et al.* (2019) Variants in DOCK3 cause developmental delay and hypotonia. *Eur. J. Hum. Genet.*, **27**, 1225–1234.
14. Alexander, M.S., Casar, J.C., Motohashi, N., Vieira, N.M., Eisenberg, I., Marshall, J.L., Gasperini, M.J., Lek, A., Myers, J.A., Estrella, E.A. *et al.* (2014) MicroRNA-486–dependent modulation of DOCK3/PTEN/AKT signaling pathways improves muscular dystrophy–associated symptoms. *J. Clin. Invest.*, **124**, 2651–2667.
15. Alexander, M., Casar, J.C., Motohashi, N., Myers, J., Eisenberg, I., Gonzalez, R., Estrella, E., Kang, P., Kawahara, G. and Kunkel, L. (2011) Regulation of DMD pathology by an ankyrin-encoded miRNA. *Skelet. Muscle*, **1**, 27.
16. Quinn, M.E., Goh, Q., Kurosaka, M., Gamage, D.G., Petrany, M.J., Prasad, V. and Millay, D.P. (2017) Myomerger induces fusion of non-fusogenic cells and is required for skeletal muscle development. *Nat. Commun.*, **8**, 15665.
17. Bi, P., McAnally, J.R., Shelton, J.M., Sánchez-Ortiz, E., Bassel-Duby, R. and Olson, E.N. (2018) Fusogenic micropeptide Myomixer is essential for satellite cell fusion and muscle regeneration. *Proc. Natl. Acad. Sci.*, **115**, 3864–3869.
18. Zhang, Q., Vashisht, A.A., O'Rourke, J., Corbel, S.Y., Moran, R., Romero, A., Miraglia, L., Zhang, J., Durrant, E., Schmedt, C. *et al.* (2017) The microprotein minion controls cell fusion and muscle formation. *Nat. Commun.*, **8**, 15664.
19. Im, W.B., Phelps, S.F., Copen, E.H., Adams, E.G., Slightom, J.L. and Chamberlain, J.S. (1996) Differential expression of

dystrophin isoforms in strains of mdx mice with different mutations. *Hum. Mol. Genet.*, **5**, 1149–1153.
20. Beastrom, N., Lu, H., Macke, A., Canan, B.D., Johnson, E.K., Penton, C.M., Kaspar, B.K., Rodino-Klapac, L.R., Zhou, L., Janssen, P.M.L. *et al.* (2011) mdx5cv mice manifest more severe muscle dysfunction and diaphragm force deficits than do mdx mice. *Am. J. Pathol.*, **179**, 2464–2474.
21. Berger, J., Berger, S., Hall, T.E., Lieschke, G.J. and Currie, P.D. (2010) Dystrophin-deficient zebrafish feature aspects of the Duchenne muscular dystrophy pathology. *Neuromuscul. Disord.*, **20**, 826–832.
22. Li, M., Hromowyk, K.J., Amacher, S.L. and Currie, P.D. (2017) The Zebrafish: Disease Models and Chemical Screens. In Detrich, H.W., Westerfield, M. and Zon, L.I. (eds), *Methods in Cell Biology*. Academic Press, Amersterdam, Netherlands, Vol. **138**, pp. 347–380.
23. Berger, J. and Currie, P.D. (2012) Zebrafish models flex their muscles to shed light on muscular dystrophies. *Dis. Models Mech.*, **5**, 726–732.
24. Bassett, D. and Currie, P.D. (2004) Identification of a zebrafish model of muscular dystrophy. *Clin. Exp. Pharmacol. Physiol.*, **31**, 537–540.
25. Bassett, D.I., Bryson-Richardson, R.J., Daggett, D.F., Gautier, P., Keenan, D.G. and Currie, P.D. (2003) Dystrophin is required for the formation of stable muscle attachments in the zebrafish embryo. *Development*, **130**, 5851–5860.
26. Jin, H., Tan, S., Hermanowski, J., Böhm, S., Pacheco, S., McCauley, J.M., Greener, M.J., Hinits, Y., Hughes, S.M., Sharpe, P.T. *et al.* (2007) The dystrotelin, dystrophin and dystrobrevin superfamily: new paralogues and old isoforms. *BMC Genomics*, **8**, 19.
27. Kawahara, G., Karpf, J.A., Myers, J.A., Alexander, M.S., Guyon, J.R. and Kunkel, L.M. (2011) Drug screening in a zebrafish model of Duchenne muscular dystrophy. *Proc. Natl. Acad. Sci.*, **108**, 5331–5336.
28. Guyon, J.R., Mosley, A.N., Zhou, Y., O'Brien, K.F., Sheng, X., Chiang, K., Davidson, A.J., Volinski, J.M., Zon, L.I. and Kunkel, L.M. (2003) The dystrophin associated protein complex in zebrafish. *Hum. Mol. Genet.*, **12**, 601–615.
29. Berger, J., Sztal, T. and Currie, P.D. (2012) Quantification of birefringence readily measures the level of muscle damage in zebrafish. *Biochem. Biophys. Res. Commun.*, **423**, 785–788.
30. Blau, H.M., Webster, C. and Pavlath, G.K. (1983) Defective myoblasts identified in Duchenne muscular dystrophy. *Proc. Natl. Acad. Sci.*, **80**, 4856–4860.
31. Blau, H.M., Webster, C., Chiu, C.-P., Guttman, S. and Chandler, F. (1983) Differentiation properties of pure populations of human dystrophic muscle cells. *Exp. Cell Res.*, **144**, 495–503.
32. Chrousos, G.P. (2016) Part 5 - Diabetes Mellitus. In Jameson, J.L., De Groot, L.J., de Kretser, D.M., Giudice, L.C., Grossman, A.B., Melmed, S., Potts, J.T. and Weir, G.C. (eds), *Endocrinology: Adult and Pediatric (Seventh Edition)*. W.B. Saunders, Philadelphia, pp. 1727–1740.e1725.
33. Dunn, J.F. and Zaim-Wadghiri, Y. (1999) Quantitative magnetic resonance imaging of the mdx mouse model of Duchenne muscular dystrophy. *Muscle Nerve*, **22**, 1367–1371.
34. Pratt, S.J.P., Xu, S., Mullins, R.J. and Lovering, R.M. (2013) Temporal changes in magnetic resonance imaging in the mdx mouse. *BMC Res. Notes*, **6**, 262.
35. Bostock, E.L., Edwards, B.T., Jacques, M.F., Pogson, J.T.S., Reeves, N.D., Onambele-Pearson, G.L. and Morse, C.I. (2018) Impaired glucose tolerance in adults with Duchenne and Becker muscular dystrophy. *Nutrients*, **10**, 1947.
36. Brazeau, G.A., Mathew, M. and Entrikin, R.K. (1992) Serum and organ indices of the mdx dystrophic mouse. *Res. Commun. Chem. Pathol. Pharmacol.*, **77**, 179–189.
37. Stapleton, D.I., Lau, X., Flores, M., Trieu, J., Gehrig, S.M., Chee, A., Naim, T., Lynch, G.S. and Koopman, R. (2014) Dysfunctional muscle and liver glycogen metabolism in mdx dystrophic mice. *PLoS One*, **9**, e91514.
38. Ahmad, N., Welch, I., Grange, R., Hadway, J., Dhanvantari, S., Hill, D., Lee, T.-Y. and Hoffman, L.M. (2011) Use of imaging biomarkers to assess perfusion and glucose metabolism in the skeletal muscle of dystrophic mice. *BMC Musculoskelet. Disord.*, **12**, 127.
39. Mokhtarian, A. and Even, P.C. (1996) Effect of intraperitoneal injection of glucose on glucose oxidation and energy expenditure in the mdx mouse model of Duchenne muscular dystrophy. *Pflugers Arch.*, **432**, 379.
40. Even, P.C., Decrouy, A. and Chinet, A. (1994) Defective regulation of energy metabolism in mdx mouse skeletal muscles. *Biochem. J.*, **304**, 649–654.
41. Kaipa, B.R., Shao, H., Schäfer, G., Trinkewitz, T., Groth, V., Liu, J., Beck, L., Bogdan, S., Abmayr, S.M. and Önel, S.-F. (2013) Dock mediates scar- and WASp-dependent actin polymerization through interaction with cell adhesion molecules in founder cells and fusion-competent myoblasts. *J. Cell Sci.*, **126**, 360–372.
42. Namekata, K., Harada, C., Taya, C., Guo, X., Kimura, H., Parada, L.F. and Harada, T. (2010) Dock3 induces axonal outgrowth by stimulating membrane recruitment of the WAVE complex. *Proc. Natl. Acad. Sci.*, **107**, 7586–7591.
43. Yajima, H. and Kawakami, K. (2016) Low Six4 and Six5 gene dosage improves dystrophic phenotype and prolongs life span of mdx mice. *Develop. Growth Differ.*, **58**, 546–561.
44. Guo, D., Peng, Y., Wang, L., Sun, X., Wang, X., Liang, C., Yang, X., Li, S., Xu, J., Ye, W.-C. *et al.* (2019) Autism-like social deficit generated by Dock4 deficiency is rescued by restoration of Rac1 activity and NMDA receptor function. *Mol. Psychiatry*. doi: 10.1038/s41380-019-0472-7.
45. Namekata, K., Enokido, Y., Iwasawa, K. and Kimura, H. (2004) MOCA induces membrane spreading by activating Rac1. *J. Biol. Chem.*, **279**, 14331–14337.
46. Namekata, K., Harada, C., Guo, X., Kimura, A., Kittaka, D., Watanabe, H. and Harada, T. (2012) Dock3 stimulates axonal outgrowth via GSK-3β-mediated microtubule assembly. *J. Neurosci.*, **32**, 264–274.
47. Yang, W.-H., Lan, H.-Y., Huang, C.-H., Tai, S.-K., Tzeng, C.-H., Kao, S.-Y., Wu, K.-J., Hung, M.-C. and Yang, M.-H. (2012) RAC1 activation mediates Twist1-induced cancer cell migration. *Nat. Cell Biol.*, **14**, 366–374.
48. Vieira, N.M., Spinazzola, J.M., Alexander, M.S., Moreira, Y.B., Kawahara, G., Gibbs, D.E., Mead, L.C., Verjovski-Almeida, S., Zatz, M. and Kunkel, L.M. (2017) Repression of phosphatidylinositol transfer protein α ameliorates the pathology of Duchenne muscular dystrophy. *Proc. Natl. Acad. Sci.*, **114**, 6080–6085.
49. Oak, S.A., Zhou, Y.W. and Jarrett, H.W. (2003) Skeletal muscle signaling pathway through the dystrophin glycoprotein complex and Rac1. *J. Biol. Chem.*, **278**, 39287–39295.
50. Chockalingam, P.S., Cholera, R., Oak, S.A., Zheng, Y., Jarrett, H.W. and Thomason, D.B. (2002) Dystrophin-glycoprotein complex and Ras and rho GTPase signaling are altered in muscle atrophy. *Am. J. Physiol. Cell Physiol.*, **283**, C500–C511.

51. Heller, H., Gredinger, E. and Bengal, E. (2001) Rac1 inhibits myogenic differentiation by preventing the complete withdrawal of myoblasts from the cell cycle. *J. Biol. Chem.*, **276**, 37307–37316.
52. Bai, Y., Guo, D., Sun, X., Tang, G., Liao, T., Peng, Y., Xu, J. and Shi, L. (2018) Balanced Rac1 activity controls formation and maintenance of neuromuscular acetylcholine receptor clusters. *J. Cell Sci.*, **131**, jcs215251.
53. Samson, T., Will, C., Knoblauch, A., Sharek, L., von der Mark, K., Burridge, K. and Wixler, V. (2007) Def-6, a guanine nucleotide exchange factor for Rac1, interacts with the skeletal muscle integrin chain α7A and influences myoblast differentiation. *J. Biol. Chem.*, **282**, 15730–15742.
54. Vieira, N.M., Elvers, I., Alexander, M.S., Moreira, Y.B., Eran, A., Gomes, J.P., Marshall, J.L., Karlsson, E.K., Verjovski-Almeida, S., Lindblad-Toh, K. *et al.* (2015) Jagged 1 rescues the Duchenne muscular dystrophy phenotype. *Cell*, **163**, 1204–1213.
55. Thisse, C. and Thisse, B. (2008) High-resolution in situ hybridization to whole-mount zebrafish embryos. *Nat. Protocols*, **3**, 59–69.
56. Wildforster, V. and Dekomien, G. (2009) Detecting copy number variations in autosomal recessive limb-girdle muscular dystrophies using a multiplex ligation-dependent probe amplification (MLPA) assay. *Mol. Cell. Probes*, **23**, 55–59.
57. Hightower, R.M., Reid, A.L., Gibbs, D.E., Wang, Y., Widrick, J.J., Kunkel, L.M., Kastenschmidt, J.M., Villalta, S.A., van Groen, T. and Chang, H. (2020) The SINE compound KPT-350 blocks dystrophic pathologies in DMD zebrafish and mice. *Mol. Ther.*, **28**, 189–201.
58. Schindelin, J., Arganda-Carreras, I., Frise, E., Kaynig, V., Longair, M., Pietzsch, T., Preibisch, S., Rueden, C., Saalfeld, S., Schmid, B. *et al.* (2012) Fiji: an open-source platform for biological-image analysis. *Nat. Methods*, **9**, 676–682.
59. Ahrens, H.E., Henze, H., Schüler, S.C., Schmidt, M., Hüttner, S.S. and von Maltzahn, J. (2019) Analyzing satellite cell function during skeletal muscle regeneration by cardiotoxin injury and injection of self-delivering siRNA in vivo. *J. Vis. Exp.* doi: 10.3791/6019.
60. Koster, J. and Rahmann, S. (2012) Snakemake–a scalable bioinformatics workflow engine. *Bioinformatics*, **28**, 2520–2522.
61. Patro, R., Duggal, G., Love, M.I., Irizarry, R.A. and Kingsford, C. (2017) Salmon provides fast and bias-aware quantification of transcript expression. *Nat. Methods*, **14**, 417–419.
62. Ewels, P., Magnusson, M., Lundin, S. and Kaller, M. (2016) MultiQC: summarize analysis results for multiple tools and samples in a single report. *Bioinformatics*, **32**, 3047–3048.
63. Soneson, C., Love, M.I. and Robinson, M.D. (2015) Differential analyses for RNA-seq: transcript-level estimates improve gene-level inferences. *F1000Res*, **4**, 1521.
64. Love, M.I., Huber, W. and Anders, S. (2014) Moderated estimation of fold change and dispersion for RNA-seq data with DESeq2. *Genome Biol.*, **15**, 550.
65. Livak, K.J. and Schmittgen, T.D. (2001) Analysis of relative gene expression data using real-time quantitative PCR and the 2-[Delta][Delta]CT method. *Methods*, **25**, 402–408.
66. Cheung, T.H., Quach, N.L., Charville, G.W., Liu, L., Park, L., Edalati, A., Yoo, B., Hoang, P. and Rando, T.A. (2012) Maintenance of muscle stem-cell quiescence by microRNA-489. *Nature*, **482**, 524–528.
67. Gharaibeh, B., Lu, A., Tebbets, J., Zheng, B., Feduska, J., Crisan, M., Peault, B., Cummins, J. and Huard, J. (2008) Isolation of a slowly adhering cell fraction containing stem cells from murine skeletal muscle by the preplate technique. *Nat. Protocols*, **3**, 1501–1509.
68. Alexander, M.S., Kawahara, G., Motohashi, N., Casar, J.C., Eisenberg, I., Myers, J.A., Gasperini, M.J., Estrella, E.A., Kho, A.T., Mitsuhashi, S. *et al.* (2013) MicroRNA-199a is induced in dystrophic muscle and affects WNT signaling, cell proliferation, and myogenic differentiation. *Cell Death Differ.*, **20**, 1194–1208.
69. Leikina, E., Gamage, D.G., Prasad, V., Goykhberg, J., Crowe, M., Diao, J., Kozlov, M.M., Chernomordik, L.V. and Millay, D.P. (2018) Myomaker and Myomerger work independently to control distinct steps of membrane remodeling during myoblast fusion. *Dev. Cell*, **46**, 767–780.e767.
70. Vadivelu, S.K., Kurzbauer, R., Dieplinger, B., Zweyer, M., Schafer, R., Wernig, A., Vietor, I. and Huber, L.A. (2004) Muscle regeneration and myogenic differentiation defects in mice lacking TIS7. *Mol. Cell. Biol.*, **24**, 3514–3525.
71. Sievers, F. and Higgins, D.G. (2018) Clustal omega for making accurate alignments of many protein sequences. *Protein Sci.*, **27**, 135–145.